Analytical Methods

# Characterization of low adsorption filter membranes for electrophoresis and electrokinetic sample manipulations in microfluidic paper-based analytical devices



| | |
|---|---|
| Journal: | *Analytical Methods* |
| Manuscript ID | AY-ART-05-2018-001237.R1 |
| Article Type: | Paper |
| Date Submitted by the Author: | 29-Jun-2018 |
| Complete List of Authors: | Casto, Laura; University of Tennessee, Chemistry<br>Schuster, Jennifer; University of Tennessee, Chemistry<br>Neice, Claire; Virginia Polytechnic Institute and State University, Chemistry; University of Tennessee, Chemistry<br>Baker, Christopher; University of Tennessee, Chemistry |
| | |

Research article prepared for submission to:
*Analytical Methods*

# Characterization of low adsorption filter membranes for electrophoresis and electrokinetic sample manipulations in microfluidic paper-based analytical devices

Laura D. Casto, Jennifer A. Schuster, Claire D. Neice, Christopher A. Baker*

Department of Chemistry, University of Tennessee, Knoxville, 552 Buehler Hall, 1420 Circle Dr., Knoxville, TN 37996

Keywords: Paper microfluidics, μPAD, microfabrication, separation, zonal electrophoresis

*Address correspondence to:
Dr. Christopher A. Baker
Department of Chemistry
University of Tennessee, Knoxville
552 Buehler Hal
1420 Circle Dr.
Knoxville, TN 37996
Phone: (865)974-8225
Email: chris.baker@utk.edu

**Abstract**

The emergence of microfluidic paper-based analytical devices (μPADs) has renewed interest in paper as a substrate for chemical separations and analysis. The availability of engineered filter membrane materials effectively broadens the definition of "paper" as a substrate material, and presents the opportunity to utilize their engineered properties in chemical analyses. Here we evaluate a selection of low adsorption filter membrane materials for their efficacy in achieving zonal electrophoretic separations of amino acids within μPADs. Cellulose acetate (Whatman OE66), cellulose ester (MF-Millipore), and polyvinylidene fluoride (Durapore PVDF) substrates were evaluated for their performance in electrokinetic μPADs, including establishing microfabrication parameters, characterizing Joule heating, and establishing fluorescence detection limits. Heating-limited electric fields in the range of 230 - 350 V $cm^{-1}$ were achieved, and fluorescence limits of detection of *ca.* 3 nM were observed in both green (fluorescein) and red (nile blue) fluorescence channels for OE66 substrates. Electrophoretic separations of a three amino acid mixture were demonstrated in PVDF and OE66 μPADs, while relatively high rates of electroosmotic flow in MF-Millipore substrates enabled electrokinetic flow gating in this material. These studies demonstrate the efficacy of zonal electrophoresis in μPADs made from low adsorption substrates, and highlight design considerations for the development of similar μPAD systems.

**Introduction**

Paper has a long history as a substrate for analytical separations, from the origins of paper chromatography in the 19th century,[1] to early examples of paper-supported electrophoresis in the 1930s.[2] The low cost and reduced analysis volumes achieved in paper substrates are as valuable in addressing modern analytical challenges as they were in the first half of the twentieth century, however paper was largely replaced in electrophoresis applications with the emergence of hydrogel materials like polyacrylamide,[3] and high resolution techniques such as capillary electrophoresis.[4] Subsequently, capillary electrophoresis played a role in the evolution of microfluidic lab-on-a-chip systems,[5,6] many of which utilize electroosmotic flow and other electrokinetic sample manipulations to automate sample handling and analysis.

The emergence of microfluidic paper-based analytical devices (μPADs)[7, 8] has renewed interest in paper as a substrate material for chemical analysis. Most commonly, μPADs take advantage of passive transport by capillary action in the paper substrate, which reduces cost and complexity of instrumentation. For example, a recent report describes high sensitivity detection of the cancer marker alpha-fetoprotein from human serum in a wax printed μPAD

device.[9] This device enabled an automated enzyme-labeled immunoassay, utilizing only capillary flow within the paper substrate for analyte and reagent mass transport, and achieved a detection limit of 1 ng $mL^{-1}$ (*ca.* 15 pM). In addition to lateral flow immunoassays, distance-based readout schemes are becoming popular in μPAD assay designs.[10–12] Chen et. al combined immunoassay and distance readout techniques in a μPAD to achieve detection of carcinoembryonic antigen with a 2 ng $mL^{-1}$ (*ca.* 10 pM) detection limit.[13] This device utilized a sandwich immunoassay in which capture antibodies were immobilized at the μPAD channel inlet, and excess HRP-labeled detection antibodies were washed away along a paper channel by capillary action. The length of the eluted band of detection antibodies was inversely correlated with the concentration of carcinoembryonic antigen captured in the sandwich assay. These examples illustrate that creative assay design and inventive approaches to quantitative detection are required to overcome the limited versatility of sample handling achievable using only capillary action. Increasing the versatility of fluidic transport in μPADs, therefore, may enable new approaches to assay design.

μPADs utilizing active fluidic transport by electroosmosis and electrophoresis have emerged in recent years.[14,15] For example, ion concentration polarization (ICP) has been utilized as a sample enrichment technique in several μPAD devices.[16–18] ICP occurs when an ion depletion region develops near the interface of free solution and nanoporous ion selective membranes, enabling electrophoretic focusing in localized regions of high electric field. This mechanism is particularly attractive in paper substrates since ion selective membranes are readily formed within the porous substrate by solution deposition of polymer materials like Nafion.[19] Sample enrichment is one example of how μPAD assays may become more versatile with the addition of active, electrokinetic sample transport.

A recent review by Breadmore and coworkers described the past and present landscape of electrophoresis in paper substrates, and identified a need for systematic study of substrate performance for electrokinetic sample manipulations in μPADs.[20] One promising opportunity in this area is the availability of modern engineered filter membrane materials that broaden the definition of “paper” as a substrate. The next generation of μPADs may exploit the properties of these engineered materials for new approaches to assay design and detection readout. Reduced sample adsorption on low binding filter membrane materials, for example, may offer advantages for performing zonal electrophoresis in μPADs.

Here, we evaluate a selection of low adsorption filter membranes for their performance in electrokinetic μPADs. Microfabrication procedures are established, and Joule heating characteristics are evaluated. We compare these materials for their performance in

fluorescence detection and separations by zonal electrophoresis. Finally, we demonstrate electrokinetic gating in a paper substrate with suitable electroosmotic flow characteristics.

## Materials and Methods

### *Materials and Reagents*

Whatman™ cellulose acetate membrane filters (OE 66 ST, 10404170, 0.2 μm pore size) were from GE Healthcare Life Sciences (Pittsburgh, PA). Durapore™ polyvinylidene fluoride (PVDF) membrane filters (SVLP04700, 5 μm pore size), and MF-Millipore™ mixed cellulose ester membranes (GSWP04700, 0.22 μm pore size; and SMWP04700, 5 μm pore size) were from Merck Millipore Ltd. (Tullagreen, Carrigtwohill Co. Cork, IRL). Sodium tetraborate, fluorescein disodium salt, fluorescein isothiocyanate isomer, Nile Blue A, Arginine, and Glutamine were ACROS Organics from ThermoFisher Scientific (Waltham, MA). Glycine was Fisher bioreagents brand from Fisher Scientific (Suwanee, GA). Tris(hydroxymethyl)amino-methane was from Sigma Chemical Co. (St. Louis, MO). 25 mm X 75 mm x 1.1 mm borosilicate microscope slides were purchased from Fisher Scientific (Suwanee, GA). All solutions were prepared in Milli-Q (Millipore, Bedford, MA) 18 MΩ · cm deionized water.

### *μPAD fabrication and assembly*

Paper microchannels were cut from filter membranes using a 30 W $CO_2$ direct laser writing instrument (VLS 2.3, Universal Laser Systems, Scottsdale, AZ). Filter membranes were secured at the edges to the cutting platform using clear tape to prevent substrates from moving under nitrogen flow from the laser cutting system. Microfluidic networks were designed in AutoCAD and cut on the laser cutter in vector mode. Linear energy density (LED) is given in units of J $mm^{-1}$ and is the ratio of the laser power (J $s^{-1}$) and linear speed (mm $s^{-1}$).[21] Three unique power and speed combinations were used to achieve each value of linear energy density reported. Microfabricated paper devices were imaged via stereo microscope, and dimensions were measured by pixel counting using ImageJ software.[22]

500 - 700 μm thick PDMS sheets (HT6240, Stockwell Elastomerics, Inc., Philadelphia, PA) and 1 mm thick borosilicate glass microscope slides were used to laminate the paper microchannels into a glass-PDMS-paper-PDMS-glass laminate structure (Figure 1). Binder clips provided sufficient clamping force to compress the PDMS around the paper substrate such that little or no dead volume was evident at the edge of the paper microchannel upon visual inspection via 10X microscope objective.

*Joule heating characterizations*

Linear channels with lengths ranging from 1 - 4 cm were cut from the respective substrates, assembled as described above, and filled with 15 mM borate buffer (pH 8). Electrical potential was applied across the length of the channels to give electric field strengths in the range of 0 - 700 V $cm^{-1}$. Each potential application was held until measured electrical current stabilized to within +/- 5% (typically 1 - 3 minutes), and the stable current was recorded. Plots of current versus electric field strength were prepared, and the heat-limited condition was defined as the field strength at which the coefficient of correlation for the least squares linear regression of current vs. applied potential dropped below 0.98, and continued to deteriorate with additional data points at higher field strengths.

*Fluorescence characterizations*

μPAD channels were wetted with either buffer or fluorescent dye solution, and fluorescence detection was carried out by inverted fluorescence microscope (Nikon Eclipse Ti-U, Nikon Instruments Inc., Melville, NY) using a high intensity LED for fluorescence excitation (SOLIS3C, Thorlabs, Newton, NJ), and sCMOS for image capture (Zyla 4.2, Andor USA, South Windsor, CT). Cube-mounted fluorescence filter sets were used to excite and collect green (96226, Nikon Instruments Inc., Melville, NY, $\lambda_{ex}$ = 480 nm, $\lambda_{ex}$ = 535 nm), and red (M358745 Semrock, Rochester, NY, $\lambda_{ex}$ = 635 nm, $\lambda_{ex}$ = 680 nm) fluorescence. Green fluorescent dye solution was 5 - 1000 nM fluorescein disodium salt in 10 mM TRIS buffer (pH 8). Red fluorescent dye solution was 5 - 1000 nM nile blue in 10 mM TRIS buffer (pH 8). Calibration plots were constructed from grayscale counts vs. dye concentration (see Figure S1 in the electronic supplementary information), and the limit of detection was defined as the standard deviation of the blank multiplied by three, divided by the slope of the calibration line.

*Electrophoretic separations*

Amino acids were labeled following a procedure described previously.[23] Briefly, arginine, glycine and glutamine, were combined with a limiting concentration of FITC to final concentrations of 1 mM for arginine and glutamine, and either 1 mM or 2 mM glycine and 100 μM FITC in 20 mM sodium tetraborate (pH 9.5). The variation in glycine concentration was used to help identify migration order, and limiting FITC concentration ensured that no removal of excess FITC was necessary. The reaction was protected from light, and placed on a rotator at

room temperature overnight. The concentrated solution of FITC-labeled amino acids was diluted 200-fold in 10 mM TRIS buffer (pH 8) to a final concentration of 500 nM total FITC content.

μPADs consisting of individual linear channels of 4 cm length and 1 mm in width were assembled as described above. One buffer reservoir was filled with background electrolyte (BGE) of either 10 mM TRIS, pH 8.0 or 10 mM sodium borate, pH 8.5 and the channels were left to fill by capillary action. While the channel filled, 500 nL of sample was manually pipetted onto the unwetted end of the paper channel to form the sample plug for electrophoretic separation. Fluorescence detection was carried out using the inverted microscope system illustrated in Figure 1. Peak profiles were extracted from recorded videos of migrating fluorescent bands by defining a region of interest within the paper channel using ImageJ software, and plotting grayscale intensity versus time. Baseline drift was subtracted from electropherograms using Origin Pro (OriginLab Corporation, Northampton, MA) and signal intensity values were normalized to give each electropherogram a maximum intensity of 1 relative unit.

*Electrokinetic gating*

μPADs with cross-t geometries were prepared as described above. All channels of the cross-t geometry were 1 cm in length, which simplified control of the applied field strengths in the complex geometry. Applied voltage was 400V, to achieve a field strength of 200 V $cm^{-1}$ in all channels of the device. BGE was 10 mM sodium borate, and sample was 250 nM fluorescein in BGE.

**Results**

The reemergence of paper as a substrate for chemical analysis, in the form of μPADs, presents the opportunity to utilize modern filter membrane materials for their specific engineered properties. Here, we investigated a selection of three low adsorption filter membrane materials. MF-Millipore (MF) is a hydrophilic filter membrane of mixed cellulose ester composition. Polyvinylidene fluoride (PVDF) is a polymer membrane material commonly employed in biological and analytical chemistry filtration applications. Whatman OE 66 (OE66) is a filter membrane material of cellulose acetate composition. Low adsorption filter membranes were chosen for their potential to enable electrokinetic transport minimally influenced by sample-substrate adsorption. We hypothesized that this property would enable effective zonal electrophoresis within these materials.

*μPAD fabrication*

Wax printing is a common fabrication procedure for capillary-driven μPADs. We elected instead to laser cut microchannels from the filter membrane substrates using a $CO_2$ direct write laser for two reasons: 1) Cutting away unused areas of the membrane substrate reduced the total thermal mass of the device, aiding in heat dissipation; and 2) Differences in wettability of the various membrane materials may lead to variability in channel dimensions and geometries patterned by wax printing.

Since laser cutting is an ablation process, the thermal breakdown properties of the substrate materials play a role in the resulting dimensions of the microchannels. Thus, we characterized the ablated dimension, termed the cut width, as a function of LED for the low adsorption filter membrane materials (Figure 2). For all materials a similar trend was observed, increasing cut width with increasing LED up to a maximum above which no increase is observed with increasing LED. This trend is similar to that observed with direct laser ablation of glass microfluidic channels.[21] Large variance in cut width was observed, especially in the LED regime above maximum cut width. We hypothesize that large variances originates from the substrates being thermally labile, possibly resulting in uncontrolled combustion processes at the micron scale. This effect is most pronounced in PVDF substrates. For all materials tested here, maximum cut width was achieved at LED values between 0.3 and 0.6 J $mm^{-1}$. Interestingly, in all cases the maximum observed cut width was greater than the focused spot size of the $CO_2$ laser, which was *ca.* 125 μm. This finding suggests that radiant heat occurring secondary to that within the area of laser incidence participates in the ablation of the membrane materials.

Since cut width describes the amount of paper ablated in the fabrication process, and channel dimensions are defined by the paper left behind after ablation, cut width will play a role in the lower limit of achievable channel dimensions. A theoretical lower limit can be conceived as a function of the variance of cut width and the precision of laser positioning, however the practical lower limit was encountered before the influence of these factors became evident. In practice, channels with dimensions smaller than ca. 250 μm tended to curl up and protrude into the path of the advancing laser, resulting in fabrication failure. To avoid this, all further characterizations were carried out on μPAD devices with channel widths of 1 mm.

*Joule heating characterization*

Joule heating was recognized as a limiting factor in early examples of paper electrophoresis.[24] μPADs offer similar advantages for heat management to those found in other microfabricated electrophoresis platforms; specifically, reduced current due to small channel

dimensions, reduced thermal mass, and increased heat dissipation due to increased surface area to volume ratios. The potential for poor heat conduction via the fibrous organic substrates, however, presents a unique challenge in μPADs. Plots of current vs. applied potential were used to determine the electric field strength at which Joule heating changes the conductivity of the system. Illustrated in Figure 3, Joule heating was evaluated with the μPAD channels operated in three conditions: exposed to ambient air, within the laminated μPAD, and the laminated μPAD with the addition of active cooling by a flow of cooled nitrogen.

Statistical evaluation by two way ANOVA revealed that the heating trends observed for OE66 and PVDF are statistically similar, with 95% confidence. Trends observed for $MF_5$ and $MF_{0.22}$ were also statistically similar with 95% confidence; however, the OE66/PVDF trends differed from $MF_5$/$MF_{0.22}$ trends with statistical significance at 99% confidence ($p < 1 \times 10^{-7}$). For all substrates, the limiting electric field when operated in ambient air was *ca.* 100 V $cm^{-1}$. In ambient air and at fields greater than 100 V $cm^{-1}$ all microchannels followed a similar failure mode of thermal breakdown or spontaneous ignition. Lamination of the μPAD channels improved heat dissipation, as the glass microscope slides acted as heat sinks. To observe the relative contribution of pore size to heating and heat dissipation, MF substrates were evaluated at 0.22 μm and 5 μm pore diameters, both being 75% porous ($MF_{0.22}$ and $MF_5$, respectively). In the laminated device without cooling, a decrease in the heat-limited electric field was observed for $MF_5$ as compared to $MF_{0.22}$. This difference may suggest that increased surface area within the porous substrate contributes to conductive heat dissipation, however further study is needed to isolate this heat transfer mechanism. With the addition of active cooling, differences in heat dissipation due to pore size were no longer evident, suggesting that the rate of heat transfer at the air-glass interface had a greater effect under these conditions than the rate of buffer-to-substrate heat transfer. With laminating and active cooling, heat-limited electric field strengths in the range of 230 - 350 V $cm^{-1}$ were achievable, with PVDF and OE66 performing similarly and achieving higher limiting fields than those of MF.

In general, studies of joule heating in low adsorption filter membrane μPADs demonstrated that with lamination and active cooling these devices can be operated at electric field strengths between those typical of slab gel electrophoresis (< 100 V/cm)[25] and those typical of capillary and microchannel electrophoresis (>500 V/cm).[26]

*Fluorescence characterization*

Electrophoretic separations often employ fluorescence detection, but in this regard μPADs present the challenge of scatter and autoluminescence from the opaque substrate. To

assess the potential for fluorescence detection, we characterized limits of detection for fluorescence measurements conducted within these membrane materials, illustrated in Figure 4. Fluorescence in green and red emission channels were assessed using fluorescein and nile blue, respectively. Fluorescein detection limits were 98 ± 9 nM and 41 ± 3 nM in MF and PVDF substrates, respectively. These measurements were limited by relatively high intensity of luminescence or scatter from the MF and PVDF substrate as compared with OE66, which showed a limit of detection for fluorescein of 2.7 ± 0.1 nM. We observed no indication of significant photobleaching during imaging, which involved fluorescence excitation of the sample for approximately 30 seconds per measurement. Background intensities were substantially reduced with red illumination for all substrate materials, leading to reduced nile blue detection limits as compared to fluorescein for MF and PVDF substrates (11 ± 2 nM and 4.0 ± 0.5 nM, respectively). Although background intensity was substantially reduced with red illumination of OE66, the fluorescence sensitivity, as defined by the calibration slope, was also substantially reduced for nile blue as compared to fluorescein. As a result, OE66 detection limits were slightly higher for nile blue (3.5 ± 0.3 nM) as compared to fluorescein. Importantly, reduced fluorescence sensitivity appears to be a property of the dye molecule, as reduced sensitivity was observed in all substrates for nile blue as compared to fluorescein.

As anticipated, the intensity of background luminescence presents a challenge for high sensitivity fluorescence detection in these substrate materials. Reduced background luminesce in OE66 gives an advantage for fluorescence detection in the green emission channel. Importantly, these LOD characterizations illustrate relative differences in detection limits between substrate materials, but not absolute achievable limits. Camera gain and exposure time were not optimized for maximum signal-to-noise ratios in these studies, and therefore lower absolute detection limits may be possible. Still, the trends observed here suggest OE66 is favorable for electrokinetic μPADs employing fluorescence detection.

*Electrophoresis and electrokinetic gating*

The incorporation of zonal electrophoresis into μPAD designs is expected to enable complex analyses that utilize fast, efficient, and high resolution separations. Depending on the degree of interaction, analyte-substrate adsorption within paper channels may result in peak asymmetry, band broadening, and ultimately the loss of zonal separation. To evaluate the efficacy of zonal electrophoresis in low adsorption filter membranes, a fluorescently labeled amino acid mixture of FITC-arginine, FITC-glutamine, and FITC-glycine was separated in the μPAD devices. Effective separation was not possible in MF substrates, which demonstrated

high electroosmotic flow velocities in the direction from anode to cathode. As a result, a complex and irreproducible pattern of bands was observed migrating past the detection point in under 4 minutes (see Figure S2 in the electronic supplementary information). While these rates of electroosmotic flow velocity do not preclude effective zonal electrophoresis, optimization of device geometry and applied field strength would be needed to assess the feasibility of zonal separations in MF.

Figure 5A illustrates representative amino acid separations performed in PVDF substrates using BGE of 10 mM TRIS (solid lines) or 10 mM sodium borate (dashed lines). Low rates of electroosmotic flow velocity required these separations to be conducted in the direction from cathode to anode. While zonal separation is clearly observed in the PVDF substrate using TRIS BGE, resolution is lost with sodium borate BGE. The mechanism by which resolution is lost in borate BGE is unclear, however we hypothesize that a low velocity of electroosmotic flow is present in opposition to the direction of electrophoresis. In this case, the higher ionic strength of sodium borate as compared with TRIS may reduce double layer thickness and zeta potential, as observed in other model systems,[27] thereby reducing EOF velocity. The expected result would be overall faster electromigration, as observed, and potentially reduced resolution. More work is needed to investigate this mechanism further, however this study demonstrates the importance of buffer selection for separations and other electrokinetic sample manipulations carried out within the high surface area environment of paper substrates.

Representative amino acid separations in OE66 μPADs are shown in Figure 5B. Similar to PVDF, low rates of EOF required separations to be performed in the direction from cathode to anode. Unlike PVDF, resolution is observed in both TRIS and sodium borate BGE, albeit with reduced resolution in borate. OE66 substrates are demonstrated to be less sensitive to the mechanisms that lead to degraded resolution in PVDF μPADs utilizing borate BGE.

Migration time reproducibility was substantially improved in PVDF as compared to OE66 substrates. Migration time RSDs were 12% and 19% for arginine and glutamine (leading and trailing peaks, respectively) in OE66 with TRIS BGE. In PVDF with TRIS BGE, RSDs for arginine and glutamine migration times were 3.8% and 3.4%, respectively.

Peak asymmetry calculations offer insight to the degree of analyte-substrate interactions that negatively impact zonal electrophoresis separations in these substrates. Peak asymmetry values for arginine and glycine in PVDF substrates with TRIS BGE were 2.0 ± 0.3 and 1.9 ± 0.5, respectively. In OE66 substrates with TRIS BGE, these values were 1.7 ± 0.3 for arginine, and 0.6 ± 0.5 for glycine which showed substantial peak fronting. Glycine fronting was reduced in borate BGE giving peak asymmetry values of 1.4 ± 0.1. While calculated asymmetry values for

arginine in OE66 substrates increased with borate BGE to 2.3 ± 0.4, it is unclear whether this is the result of analyte-substrate adsorption or if it emerges from reduced resolution between the principle arginine peak and a trailing shoulder observed in both BGE conditions. Overall, peak asymmetry in these experiments was somewhat higher than one would expect for ideal zonal electrophoretic separations in an open tubular format. This is to be expected, as the porous paper substrate materials contain increased surface area as compared with open tubular microfluidic devices. Still, peak asymmetry does not prevent electrophoretic resolution of the principle amino acid peaks utilized in this study.

Although high EOF velocities in MF substrates were detrimental to electrophoretic separation, electroosmotic flow is useful for achieving complex fluid transport schemes in microfluidic devices.[28] Electrokinetic gated injection is often utilized to restrict or initiate flow of a reagent in microfluidic devices. Figure 6 illustrates that EOF in MF substrates is sufficient to achieve electrokinetic gating under applied electric fields of 200 V $cm^{-1}$. Importantly, these gating manipulations required several seconds to transition between the gated (Figure 6A) and floated (Figure 6B) configurations, which is significantly longer than typical sub-second injection times achievable in glass microfluidic devices by this gating mechanism. Upon reapplication of the appropriate potential scheme, gating was re-established and a sample injection plug was observed migrating along the right hand channel (not shown), completing the conventional electrokinetic gated injection procedure. Although electrokinetic sample manipulation occured on slower time scales to those typical for glass microfluidic devices, electroosmotic flow in MF is nonetheless sufficient to facilitate electrokinetic flow gating in μPAD even under modest electric field strengths limited by Joule heating.

Direct measurements of EOF velocity are clearly needed to understand the mechanisms observed in these studies; however, such measurements are not trivial within the high surface area environment of porous substrates. While measuring migration time of a neutral dye is a straightforward approach for determining EOF velocity in capillaries,[29,30] in paper substrates the potential influence of dye-substrate partitioning is not readily isolated from EOF velocity, hindering such measurements. Attempts were made to determine EOF velocity by the buffer dilution method,[31] but these studies were not conclusive due to irregular and irreproducible current drift observed during these experiments. As a result direct observation of EOF velocities was not achieved in this work, warranting further study.

## Conclusion

To increase the versatility of sample handling and assay design in μPADs, we evaluated the electrokinetic and electrophoretic performance of μPADs fabricated from low adsorption filter membrane substrates. The Joule heating-limited electric fields achieved in these μPADs were lower than those typical for open-tubular glass microfluidic devices, however zonal electrophoresis and electrokinetic flow gating were possible even at modest electric field strengths. Low adsorption membrane materials were considered for their potential to enable zonal electrophoretic separations minimally perturbed by the effects of analyte-substrate adsorption. Peak asymmetry observed in these studies suggest that detrimental analyte-substrate interactions do occur in these substrates, but they are not sufficient to prevent resolution of the model amino acid mixture employed in these studies. In comparing the selection of low adsorption filter membrane materials studied here, OE66 offers clear advantages for fluorescence detection and electrophoretic separation. MF demonstrates a substantial degree of electroosmotic flow, which may be useful in designing electrokinetic sample transport schemes in μPADs, but will likely require design optimization to achieve zonal electrophoretic separations.

While the present work is not exhaustive in surveying all available low adsorption filter membrane materials, these studies lend design insights toward the development of new μPAD technologies that utilize electrokinetic sample manipulations and electrophoretic separations to achieve increased complexity of analysis from low cost microfluidic instrumentation.

## Conflicts of interest

The authors declare there are no conflicts of interest

## Acknowledgements

This work was supported in part by a Joint Directed Research and Development grant from the Science Alliance at the University of Tennessee, and by laboratory start up funds from the University of Tennessee. C.D. Neice was supported by the National Science Foundation REU program under grant number CHE 1560033.

## References

1 L. S. Ettre, *Chromatographia*, 2001, **54**, 409–414.
2 A. Tiselius, *Transactions of the Faraday Society*, 1937, **33**, 524.
3 W. J. Evans, W. B. Carney, J. M. Dechary and A. M. Altschul, *Arch. Biochem. Biophys.*, 1962, **96**, 233–239.
4 J. Jorgenson and K. Lukacs, *Science*, 1983, **222**, 266–272.
5 A. Manz, D. J. Harrison, E. M. J. Verpoorte, J. C. Fettinger, A. Paulus, H. Lüdi and H. M.

Widmer, *J. Chromatogr. A*, 1992, **593**, 253–258.
6 S. C. Jacobson, L. B. Koutny, R. Hergenroeder, A. W. Moore and J. Michael. Ramsey, *Anal. Chem.*, 1994, **66**, 3472–3476.
7 A. W. Martinez, S. T. Phillips, M. J. Butte and G. M. Whitesides, *Angew. Chem. Int. Ed Engl.*, 2007, **46**, 1318–1320.
8 T. Akyazi, L. Basabe-Desmonts and F. Benito-Lopez, *Anal. Chim. Acta*, 2018, **1001**, 1–17.
9 P. Preechakasedkit, W. Siangproh, N. Khongchareonporn, N. Ngamrojanavanich and O. Chailapakul, *Biosens. Bioelectron.*, 2018, **102**, 27–32.
10 D. M. Cate, W. Dungchai, J. C. Cunningham, J. Volckens and C. S. Henry, *Lab Chip*, 2013, **13**, 2397–2404.
11 K. Yamada, T. G. Henares, K. Suzuki and D. Citterio, *ACS Appl. Mater. Interfaces*, 2015, **7**, 24864–24875.
12 X. Wei, T. Tian, S. Jia, Z. Zhu, Y. Ma, J. Sun, Z. Lin and C. J. Yang, *Anal. Chem.*, 2016, **88**, 2345–2352.
13 Y. Chen, W. Chu, W. Liu and X. Guo, *Sens. Actuators B Chem.*, 2018, **260**, 452–459.
14 L. Ge, S. Wang, S. Ge, J. Yu, M. Yan, N. Li and J. Huang, *Chem. Commun.* , 2014, **50**, 5699.
15 P. Mandal, R. Dey and S. Chakraborty, *Lab Chip*, 2012, **12**, 4026.
16 D.-T. Phan, S. A. M. Shaegh, C. Yang and N.-T. Nguyen, *Sens. Actuators B Chem.*, 2016, **222**, 735–740.
17 S.-H. Yeh, K.-H. Chou and R.-J. Yang, *Lab Chip*, 2016, **16**, 925–931.
18 S. I. Han, K. S. Hwang, R. Kwak and J. H. Lee, *Lab Chip*, 2016, **16**, 2219–2227.
19 X. Li, Y. Niu, Y. Chen, D. Wu, L. Yi and X. Qiu, *Micromachines*, 2016, **7**, 199.
20 P. Nanthasurasak, J. M. Cabot, H. H. See, R. M. Guijt and M. C. Breadmore, *Anal. Chim. Acta*, 2017, **985**, 7–23.
21 C. A. Baker, R. Bulloch and M. G. Roper, *Anal. Bioanal. Chem.*, 2011, **399**, 1473–1479.
22 C. A. Schneider, W. S. Rasband and K. W. Eliceiri, *Nat. Methods*, 2012, **9**, 671–675.
23 Y. F. Cheng and N. J. Dovichi, *Science*, 1988, **242**, 562–564.
24 H. G. Kunkel, *J. Gen. Physiol.*, 1951, **35**, 89–118.
25 B. Akerman, M. Jonsson, B. Nordén and M. Lalande, *Biopolymers*, 1989, **28**, 1541–1571.
26 S. Hjertén, L. Valtcheva, K. Elenbring and J. L. Liao, *Electrophoresis*, 1995, **16**, 584–594.
27 M. G. Carneiro-da-Cunha, M. A. Cerqueira, B. W. S. Souza, J. A. Teixeira and A. A. Vicente, *Carbohydr. Polym.*, 2011, **85**, 522–528.
28 C. A. Baker and M. G. Roper, *J. Chromatogr. A*, 2010, **1217**, 4743–4748.
29 K. Kenndler-Blachkolm, Š. Popelka, B. Gaš and E. Kenndler, *J. Chromatogr. A*, 1996, **734**, 351–356.
30 A. Hellqvist, Y. Hedeland and C. Pettersson, *Electrophoresis*, 2013, **34**, 3252–3259.
31 X. Huang, M. J. Gordon and R. N. Zare, *Anal. Chem.*, 1988, **60**, 1837–1838.

**Figures**

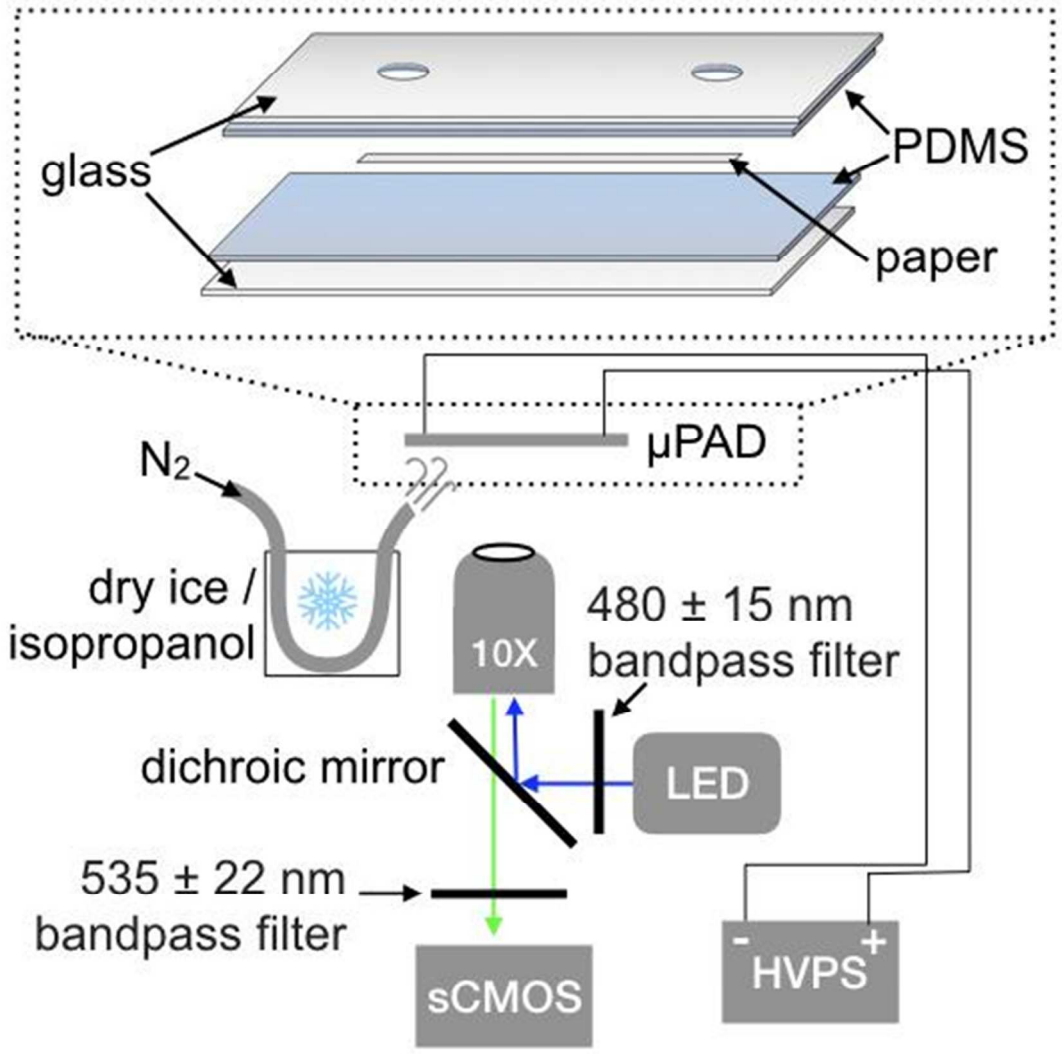


**Figure 1.** ***Schematic diagram of experimental apparatus.***
The laminated μPAD device (inset, top) was imaged on the stage of an inverted fluorescence microscope via 10X objective. A broadband light-emitting diode source provided fluorescence excitation, with emission collected by sCMOS camera. A high voltage power supply (HVPS) was used to apply electrical potential. Active cooling was accomplished using nitrogen flow cooled via dry ice and isopropanol bath. The green fluorescent filter set shown was utilized in all experiments, with an alternate red fluorescent filter set (not shown) used to determine fluorescent limits of detection for nile blue.

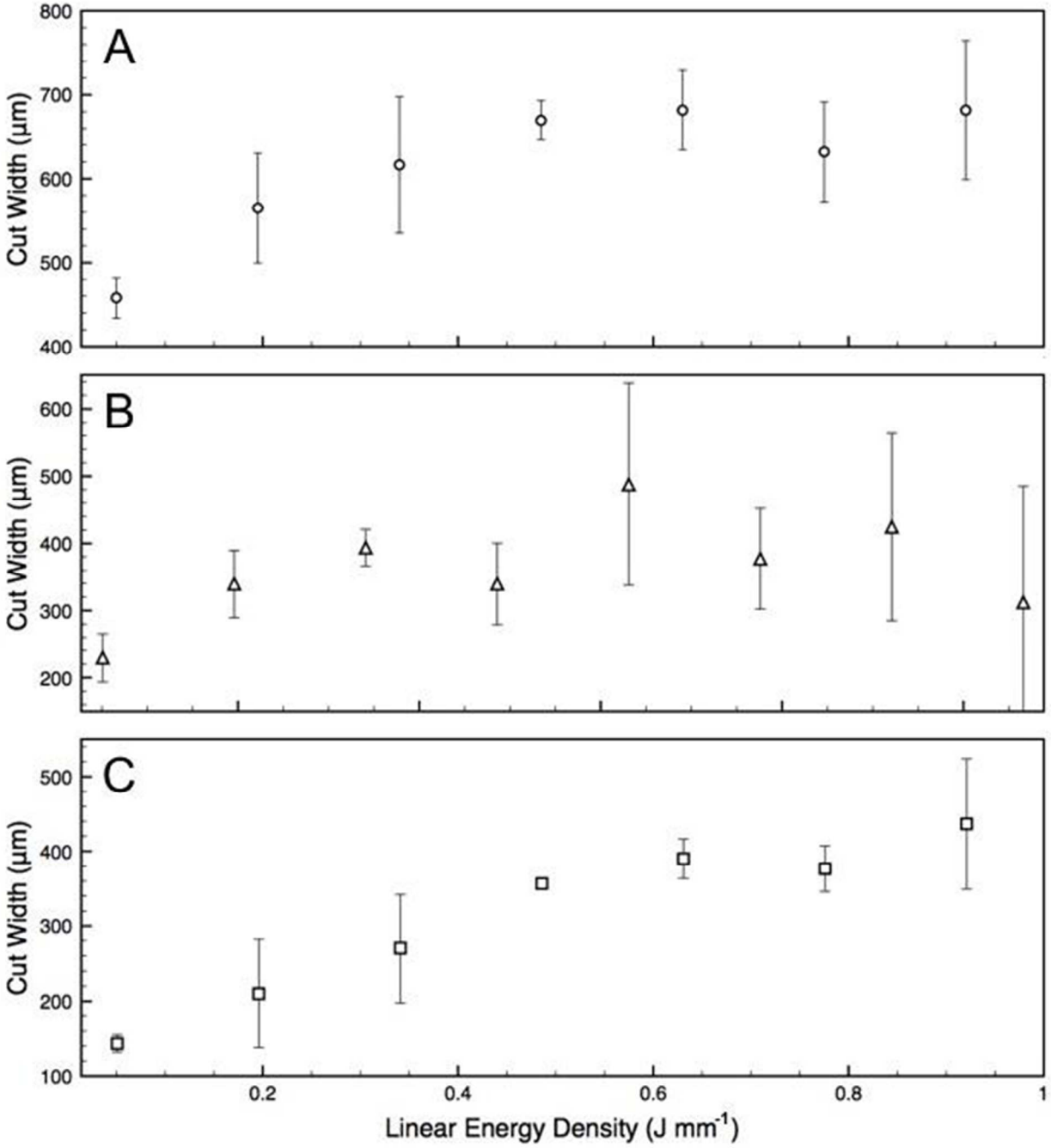


**Figure 2.** ***Characterization of laser ablation.***
Cut width as a function of linear energy density was evaluated for **A.** MF; **B.** PVDF; and **C.** OE66. Cut width was determined via digital imaging and pixel counting. Maximum cut width was observed between 0.3 and 0.6 J $mm^{-1}$ for all materials, above which ablated dimension do not increase. Error bars represent ± 1 standard deviation from n ≥ 3 replicate experiments. Linear energy density was modulated by varying laser speed, laser power, or both, with 3 unique power/speed combinations at each value of linear energy density.

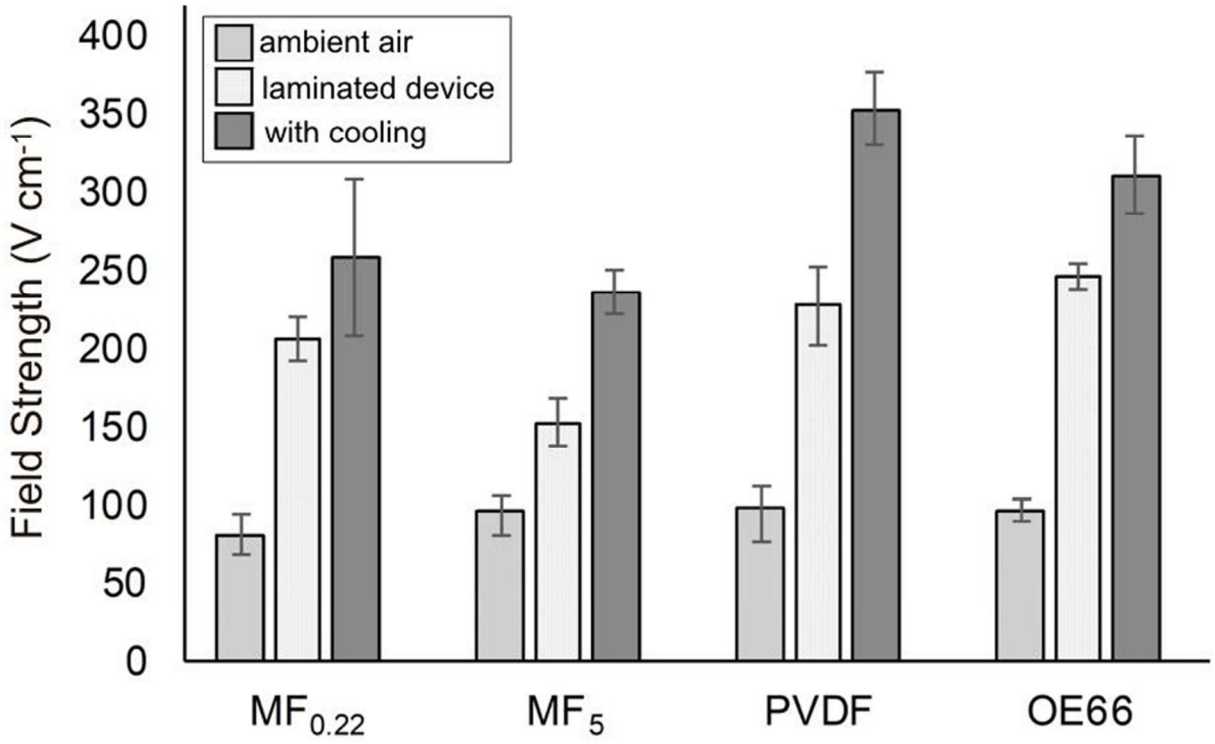


**Figure 3.** ***Joule heating-limited field strength vs. μPAD substrate material.***
Heating-limited electric field strengths were determined via plots of current vs. applied potential. "Ambient air" refers to paper channels operated in open air with no means of cooling except convective heat transfer to the ambient lab air. "Laminated device" refers to device operated in the PDMS and glass lamination illustrated in Figure 1, but without nitrogen cooling. "With cooling" refers to devices operated exactly as shown in Figure 1. MF substrates were evaluated with 0.22 and 5 μm pore sized ($MF_{0.22}$ and $MF_5$, respectively). Within each substrate, all cooling conditions are statistically different as validated by t-test ($p \leq 0.05$), except laminated and cooled conditions for $MF_{0.22}$ ($p = 0.099$). Error bars represent ± 1 standard deviation from n ≥ 3 replicate experiments.

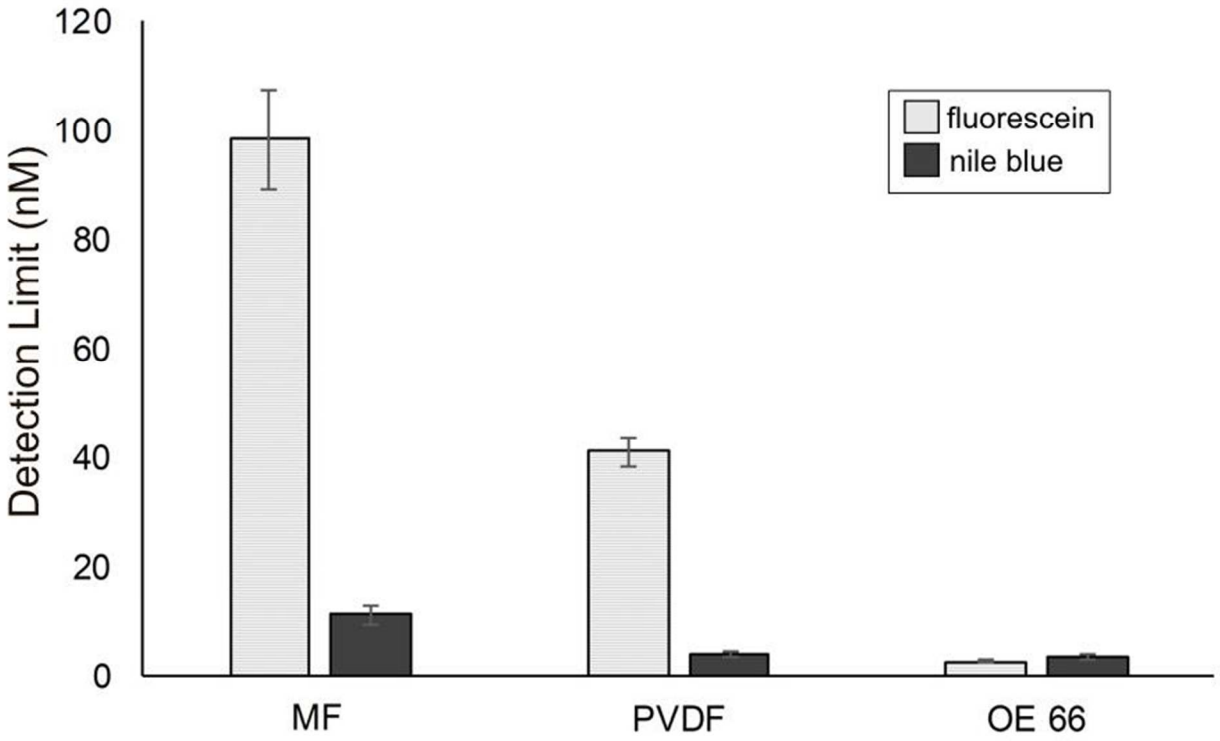


**Figure 4. Fluorescein and nile blue detection limits.**
Calibration curves were prepared using triplicate measurements in the concentration range of 0 - 500 nM fluorescent dye, and limit of detection was defined as 3X the standard deviation of the blank measurement divided by the slope of the calibration curve. Error bars represent ± 1 standard error of the estimate for the linear regression of the best fit calibration line.

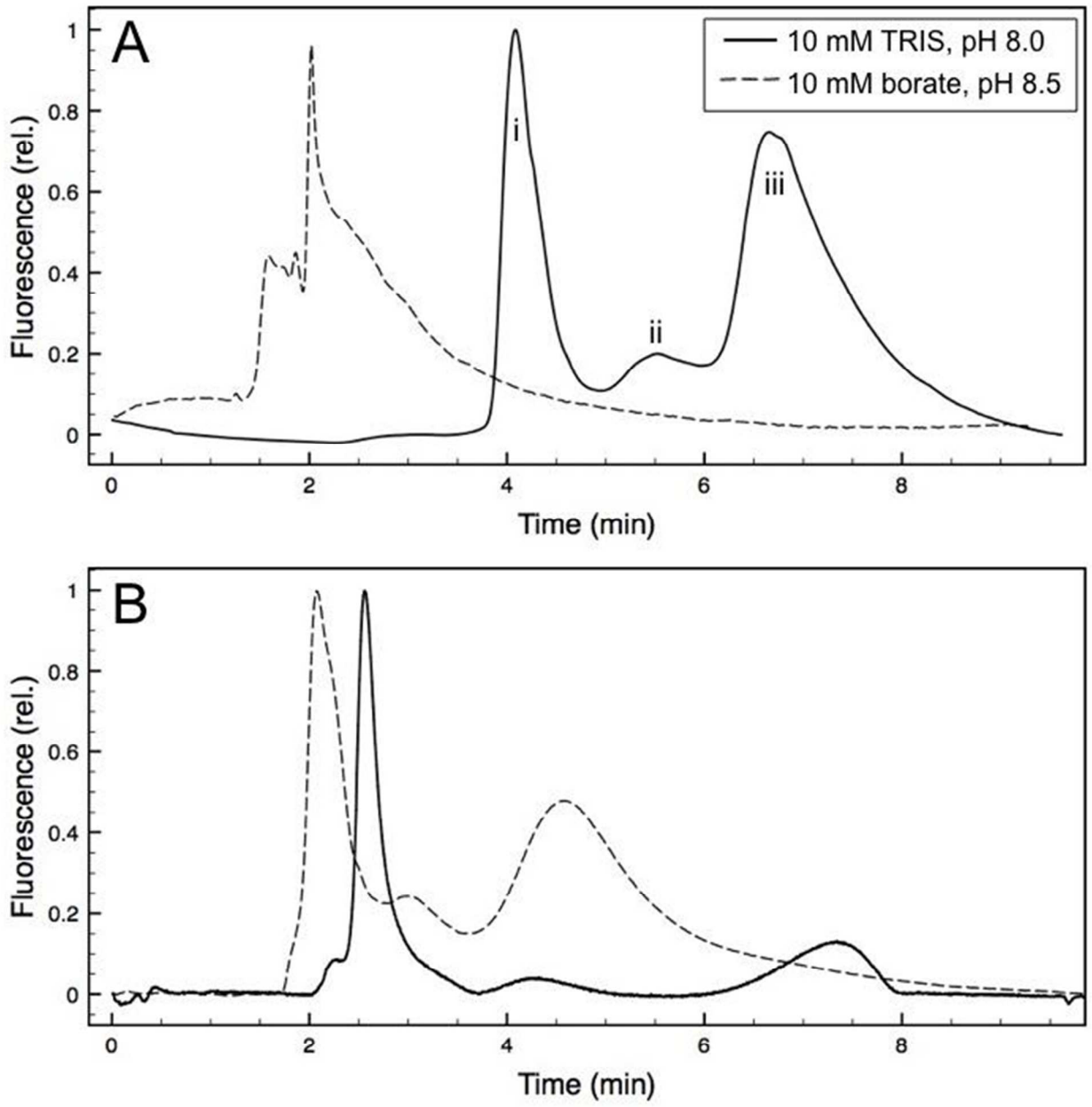


**Figure 5. Representative electropherograms in PVDF and OE66 µPADs.**
**A.** Electropherograms of arginine (i), glutamine (ii), and glycine (iii) in PVDF using TRIS (solid) or borate (dashed) BGE. **B.** The same mixture components as part A, separated in an OE66 µPAD using TRIS (solid) or borate (dashed) BGE. Fluorescence was normalized to relative units for each electropherogram.

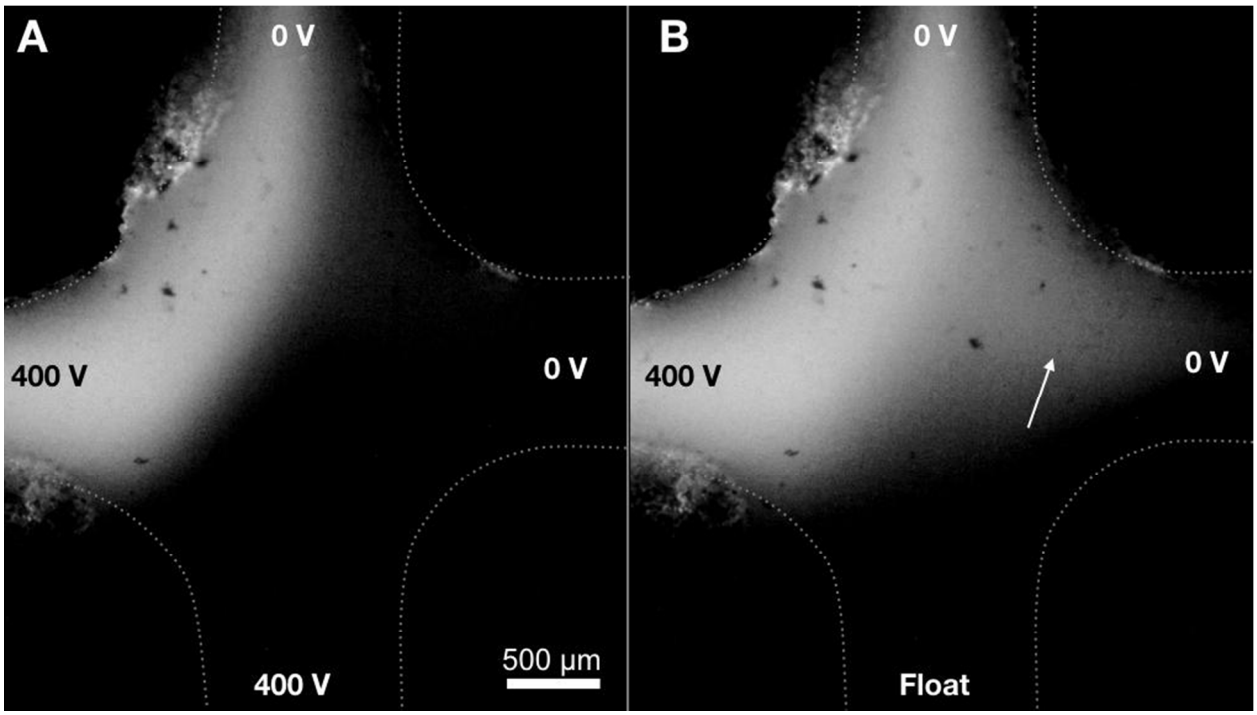


**Figure 6. Electrokinetic gating in an MF µPAD.**
Electrokinetic gating is demonstrated in a µPAD with MF substrate. **A.** In the gated configuration, under applied fields of ca. 200 V $cm^{-1}$, electroosmotic flow of buffer (from bottom) is sufficient to shunt the flow of fluorescent sample (from left) towards the top channel. **B.** In the floated configuration, potential is withheld (i.e. float potential) at the buffer inlet to allow the buildup of sample flow into the channel at the right, indicated by the arrow. Float potential was held for 4 seconds to achieve the sample flow shown here.

**Table of Contents Figure**

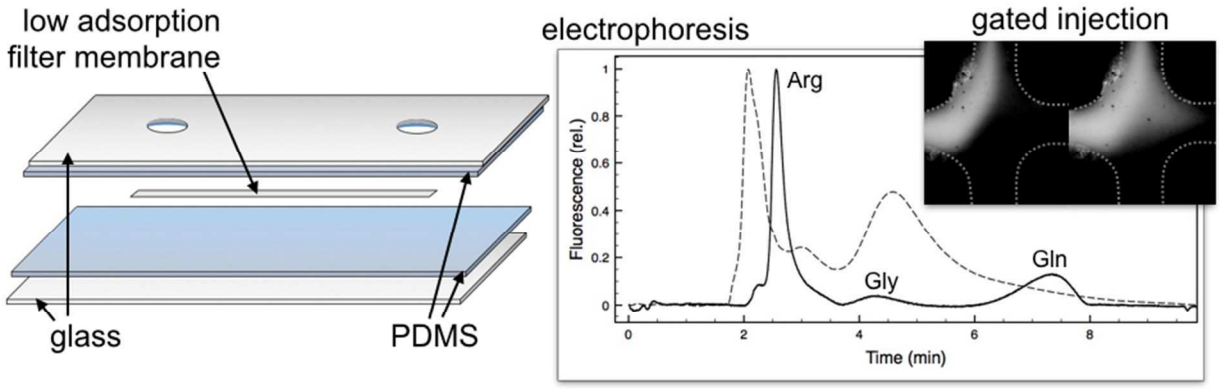


Low adsorption filter membrane materials facilitate effective zonal electrophoresis and electrokinetic gating in microfluidic paper-based analytical devices (μPADs)